



RESEARCH ARTICLE

PREPARATION, STRUCTURAL AND OPTICAL CHARACTERIZATION OF Fe DOPED
TiO₂ NANOPARTICLES

*Viruthagiri, G., Praveen, P., Shanmugam, N. and Mugundan, S.

Department of Physics, Annamalai University, Annamalainagar-608002, Tamilnadu, India

ARTICLE INFO

Article History:

Received 08th July, 2013
Received in revised form
10th August, 2013
Accepted 14th September 2013
Published online 10th October, 2013

ABSTRACT

Sol-gel method was employed in the preparation of pure and Iron (Fe- 4%, 8%, 12% & 16%) doped TiO₂ nanoparticles. The prepared Fe³⁺-TiO₂ nanoparticles were investigated by means of X-ray diffraction analysis (XRD) and UV-VIS-diffuse reflectance spectroscopy (DRS). The mono-anatase structure in the composite nanomaterials is indicated by XRD analysis. The Fe doped TiO₂ powders could apparently shift the UV-absorption band towards the higher energy region, and there was an optimal 8%Fe content in association with the larger band gap energy.

Key words:

Sol-gel; Fe-TiO₂;
XRD; UV-VIS-DRS;
Band gap

Copyright © 2013 Viruthagiri, et al., This is an open access article distributed under the Creative Commons Attribution License, which permits unrestricted use, distribution, and reproduction in any medium, provided the original work is properly cited.

INTRODUCTION

Noble metal/TiO₂ composite materials have recently emerged as candidates for numerous applications ranging from nonlinear optics to photoanode materials in solar cells, optical filtering applications and potent antimicrobial coatings [1]. There have been many reports using transition metal ion or noble metal as dopants in TiO₂ system [2]. Shah *et al.* [3] successfully used the metallorganic chemical vapour deposition method to synthesize pure TiO₂ and Pd²⁺, Pt⁴⁺ and Fe³⁺ - doped TiO₂ nanoparticles. In recent years, the modification as well as preparation and characterization of TiO₂ nanosized materials has been the focus in the semiconductor photoelectric chemistry and photocatalysis fields. Doping is used to a kind of modification method [4]. Several techniques for the synthesis of nanophase titanium dioxide have been developed so far: sol-gel processing, chemical vapour deposition, supersonic cluster beam deposition, pulsed laser deposition, etc [1]. Titanium dioxide is broadly used as a photocatalyst because; it is photochemically stable, non-toxic and cost little. Many studies [5] have been devoted to the improvement of photocatalytic efficiency of TiO₂, such as depositing noble metals and doping metal or non-metal ions. In particular, Fe³⁺-TiO₂ has been the topic of many investigation including preparation, characterization, dynamics of charge transfer, trapping and recombination, and photocatalytic behavior, etc. [5]. In our previous work, we report on the synthesis and characterization of pure [6] and Cu doped TiO₂ [7] nanostructures. In the present work, TiO₂ nanoparticles with different doping Fe³⁺ content were prepared by Sol-gel method. The structure and optical properties of the pure and Fe doped TiO₂ nanocomposites have been investigated.

Experimental

Sol-gel synthesis of Fe-TiO₂ nanoparticles: In a typical synthesis, 10 ml of tetra-isopropyl orthotitanate (TIOT, assay ≥98%) was dissolved

in 90 ml of isopropyl alcohol ((CH₃)₂-CHOH, assay >99%) and to this solution 5 ml of deionized water was added drop wise with vigorous magnetic stirring to obtain bare TiO₂. For Fe doped TiO₂, ferric nitrate nonahydrate (Fe(NO₃)₃·9H₂O, assay ≥98%) with different atomic weight percentages (4%, 8%, 12% & 16%) were added to each 10 ml of deionized water and these solutions were added drop wise to the TIOT and 2-propanol mixed solutions separately. The resulting colloidal suspensions were stirred for 4h at room temperature using magnetic stirrer. The white and pale orange gels were obtained for pure and Fe doped TiO₂, respectively. Then filtered by whatman filter paper and washed several times using ethanol and deionized water. The yield gels were dried in hot air oven at 100°C for 6h to evaporate water and organic material to the maximum extent. Then the dried powders were ground by agate mortar using pestle to remove agglomerates. Finally, the powders kept into muffle furnace and annealed at 450°C for 4h to obtain desired pure and Fe doped TiO₂ nanocrystallites. The annealed powders were pulverized to fine powders using agate mortar for further characterizations.

Characterizations: The crystalline phase and particle sizes of pure and Fe doped TiO₂ nanoparticles were analyzed by X-ray diffraction (XRD) measurement, which was carried out at room temperature by using XPERT-PRO diffractometer system (scan step of 0.05°, counting time of 10.16 s per data point) equipped with a Cu tube for generating CuKα radiation (λ = 1.5406 Å). The incident beam in the 2-theta mode over the range of 10°–80°, operated at 40 kV and 30 mA. The diffuse reflectance spectra (DRS) was measured at wavelength in the range of 200–800 nm by UV-Vis-NIR spectrophotometer (Varian/Carry 5000) equipped with an integrating sphere and the baseline correction was performed using a calibrated reference sample of powdered barium sulphate (BaSO₄).

RESULTS AND DISCUSSION

X-ray diffraction analysis: XRD characterization of pure and Fe (4%, 8%, 12% & 16%) doped TiO₂ nanoparticles are depicted in Fig.1. The

*Corresponding author: Viruthagiri, G.
Department of Physics, Annamalai University, Annamalainagar-608002,
Tamilnadu, India

peaks marked (A) and (Fe) correspond to Anatase and Iron, respectively. Diffractions that are attributable to anatase phase of TiO₂ crystals (101) are clearly detectable at $2\theta = 25.28^\circ$ (JCPDS card: 21-1272) in both the patterns of pure and Fe doped TiO₂. The orientations (101), (004), (112), (200), (105), (211), (204), (116), (220) and (215) can be assigned to the crystal planes of anatase TiO₂. Whereas, the reflections (211), (220), (110), (321), (200) and (330) can be assigned to the planes of Fe (JCPDS cards: 89-4186, 01-1267 and 01-1262). As can be seen from Fig.1, the pure and Fe doped TiO₂ samples were composed of only an anatase phase without the presence of iron oxide. It demonstrates that Fe³⁺ ions are successfully incorporated into the framework of anatase TiO₂, without the formation of iron oxide on the surface of TiO₂. All the peaks of Fe doped TiO₂ have almost the same positions from the X-axis, which were coincided well with the diffraction planes of pure TiO₂ except the characteristic peaks of iron (211), (220) and (110) (Fig.1-a, b, c & d).

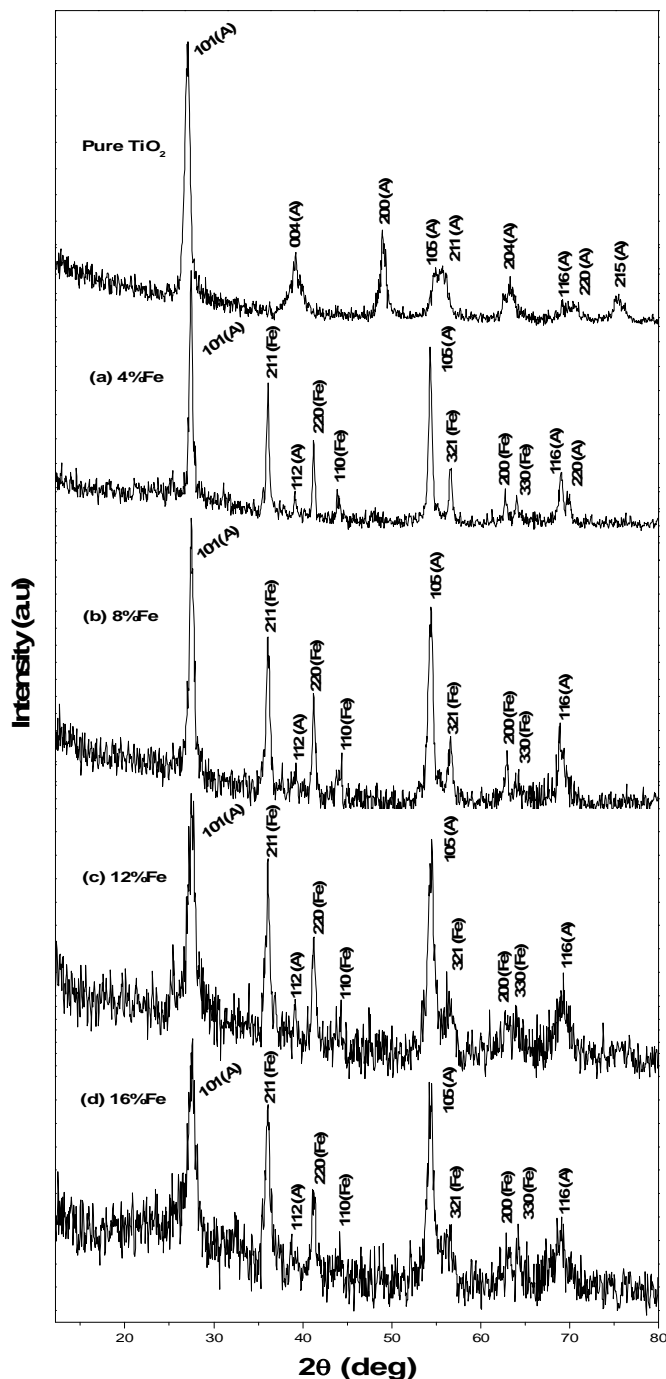


Figure 1: X-ray diffractograms of pure and Fe doped TiO₂ nanoparticles with different weight percentages (A: Anatase, Fe: Iron)

However, the peaks shifted slightly to higher 2θ values when higher amounts of iron dopant were incorporated. Its incorporation gives rise to the structural expansion of the crystalline lattice, subsequently its structural distortion. The decrease in the interplanar distance of anatase framework leads XRD peak patterns are shift to higher 2θ direction according to Bragg's law [6]. As larger amount of Fe dopant is incorporated into anatase framework, the lattice was distorted more and more. Thus, the peak shift can be regarded as indirect evidence of successful iron doping into TiO₂ crystal framework [7]. From all the diffraction patterns it is also obvious that the materials are in the form of quite small-sized nanoparticles, as the peaks are broad [8]. Hence, the new peaks appeared in Fe doped TiO₂ might be accredited to the iron content. By comparison, it can be deduced that doping Fe has a little effect on the size of anatase crystallites. The average crystallite sizes of pure and Fe doped TiO₂ nanoparticles can be estimated from the integral width of the diffraction peaks using the Scherrer formula [9]. When compared to undoped TiO₂, the peaks of 4% and 8% Fe doped TiO₂ (Fig.1-a & b) are relatively sharper which indicate that the doped ones have increased crystallite sizes. It is the manifestation of higher particle sizes than that of the pure TiO₂. Whereas, from Fig.1-c & d the XRD peaks become broader than the pristine TiO₂ attribute the smaller particle sizes. The lattice parameters *a*, *c* and *V* for the tetragonal structure can also be determined [10]. The calculated average crystallite sizes, lattice parameters of pure, and Fe doped TiO₂ nanoparticles are illustrated in Table 1. The lattice constants and cell volume of Fe doped TiO₂ nanoparticles are found increased due to the smaller ionic radius of Fe³⁺ (0.64 Å) than that of Ti⁴⁺ (0.68 Å), which indicates that the doping of Fe does not alter the tetragonal structure of anatase TiO₂. The variation of lattice constants on Fe doping with TiO₂ has plotted in Fig.2. The dominant peak is observed at (101) plane in both pure and Fe doped TiO₂ nanoparticles confirmed that the XRD peaks are attributed to tetragonal anatase phase. In fact, the XRD patterns of Fe doped TiO₂ does not considerably shift compared with bare TiO₂, suggesting that Fe does not come into the TiO₂ lattices to substitute Ti. This is possibly because of the valence difference between Fe³⁺ and Ti⁴⁺. Thus, it can be concluded that Fe is mainly dispersed on TiO₂ crystallite surfaces or located at interstitial sites [11].

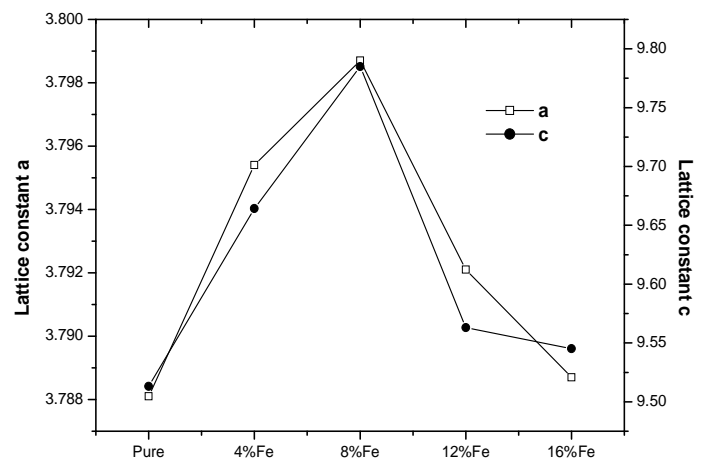


Figure 2: Variation of lattice constants for pure and Fe-TiO₂ nanoparticles

Table 1: Comparison of crystallite size and lattice parameters for pure and Fe doped TiO₂ nanoparticles

Material	Size (nm)	Lattice parameters		
		a (Å)	c (Å)	V (Å ³)
Pure TiO ₂	15.31	3.7881	9.5132	136.51
4% wt. Fe-TiO ₂	23.78	3.7954	9.6642	139.21
8% wt. Fe-TiO ₂	17.09	3.7987	9.7850	141.19
12% wt. Fe-TiO ₂	11.31	3.7921	9.5631	137.51
16% wt. Fe-TiO ₂	11.17	3.7887	9.5452	137.01

Linear optical study

Determination of band gap energy: Fig.3 shows the diffuse reflectance spectra of pure and Fe (4%, 8%, 12% & 16%) doped TiO₂ nanoparticles. Compared with pure TiO₂, the absorption edges of Fe doped TiO₂ nanoparticles shifted towards the higher energy region (i.e. blue shift) for all Fe dopant percentages. The band gap energy (E_g) of pure and Fe doped TiO₂ was obtained from the wavelength (λ) value corresponding to the intersection point of the vertical and horizontal part of the spectrum, using the equation [12]:

$$E = \frac{hc}{\lambda} \text{ eV}$$

Where h is the Planck's constant (6.626×10⁻³⁴ Js) and c is the light velocity (3×10⁸ m/s). The absorption edge of pure TiO₂ was at 345.49 nm, corresponding to band gap energy of 3.58 eV. According to the UV cut-off wavelengths 344.17, 339.15, 340.66 and 342.41 nm, the calculated band gap energies are 3.60, 3.66, 3.63 and 3.62 eV for 4%, 8%, 12% and 16% Fe doped TiO₂ nanoparticles, respectively. Hence, it can be clearly seen that the band gap energies of Fe doped TiO₂ are higher than that of pure TiO₂. The 8%Fe-TiO₂ has relatively higher band gap energy than other dopant percentages. Therefore, it has been taken for further investigation.

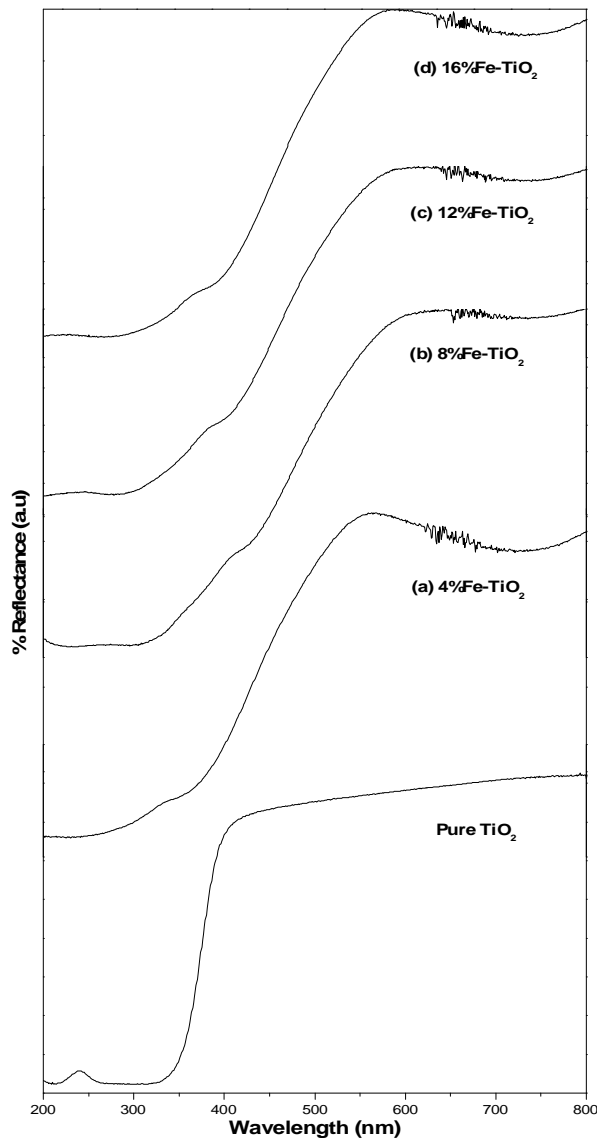


Figure 3: UV-Vis-DRS spectra of pure and Fe doped TiO₂ nanoparticles

Direct and indirect band gap energy: The absorption edge of Fe doped TiO₂ was blue-shifted about ≤6.34 nm, compared with that of

pure TiO₂. The direct band gap energy can be estimated from a plot of (αhv)² vs. photon energy (hv) by using the relationship [10],

$$\alpha hv = A (hv - E)$$

Where α = 4πk/λ (k is the absorption index or absorbance) and A is constant. The exponent n depends on the nature of the transitions; n may have values 1/2, 2, 3/2 and 3 corresponding to allowed direct, allowed indirect, forbidden direct and forbidden indirect transitions respectively. In this case n=1/2 for allowed direct transition. The plot of (αhv)² vs. hv was presented in Fig.4.

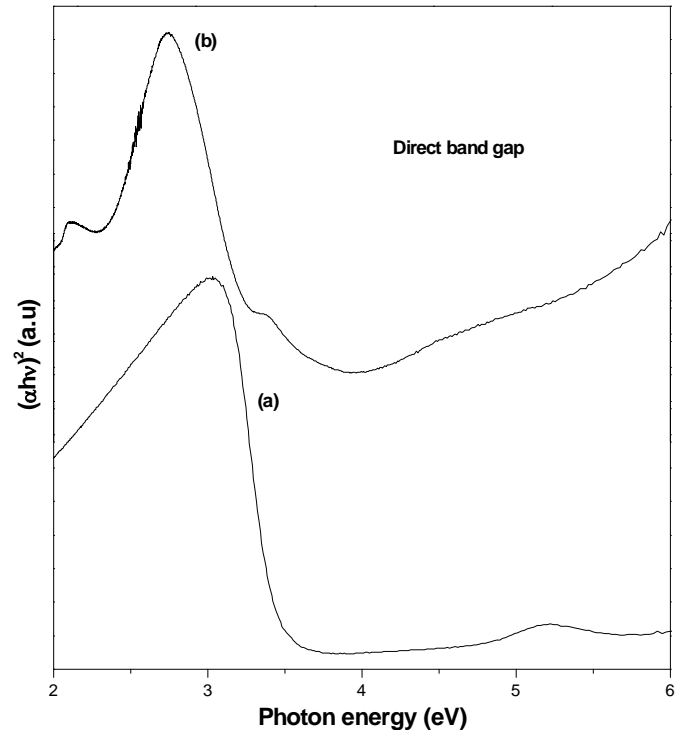


Figure 4: Plot of direct band gap energy for (a) pure and (b) 8%Fe-TiO₂ nanoparticles

The direct band gap energy of pure and 8%Fe doped TiO₂ nanoparticles were calculated to be 3.58 and 3.67 eV, respectively. Meanwhile, the crystallite size of pure TiO₂ was 15.31 nm and 8%Fe-TiO₂ was 17.09 nm (from XRD). This can be explained because the band gap energy of the materials has been found to be particle size independent, when the particle size of the materials above 10 nm they have not obey the quantum confinement effect [13]. Considering the blue shift of the absorption position from the pure TiO₂, the absorption onset be assigned to the direct transition of electrons in the Fe doped TiO₂ nanocrystals [14]. The indirect band gap energy of pure and 8%Fe doped TiO₂ nanoparticles can be estimated from plots of the square root of Kubelka Munk functions F(R) vs. hv. The reflectance data was converted to the absorption coefficient F(R) values according to the Kubelka–Munk equation [15],

$$F(R) = (1 - R) / 2R$$

Where F(R)_{KM} is equivalent to the absorption coefficient (α_{KM}), which can be expressed as,

$$\alpha (hv) = C (hv - E)$$

Where C₁ is the absorption constant for indirect transition. In this case n=2 for allowed indirect transition. The Fig.5 shows the plot of Kubelka-Munk function (i.e., relationship between (α_{KM}hv)^{1/2} and hv). The pure TiO₂ exhibits an indirect band gap value of 3.58 eV, while 8%Fe-TiO₂ exhibits the value of 3.67 eV. This result is consistent with the fact that the conduction band edge of 8%Fe-TiO₂ is about 0.09 eV

more positive than that of pure anatase TiO₂. It is evident that the pure and Fe doped TiO₂ show large optical absorbance in the UV region.

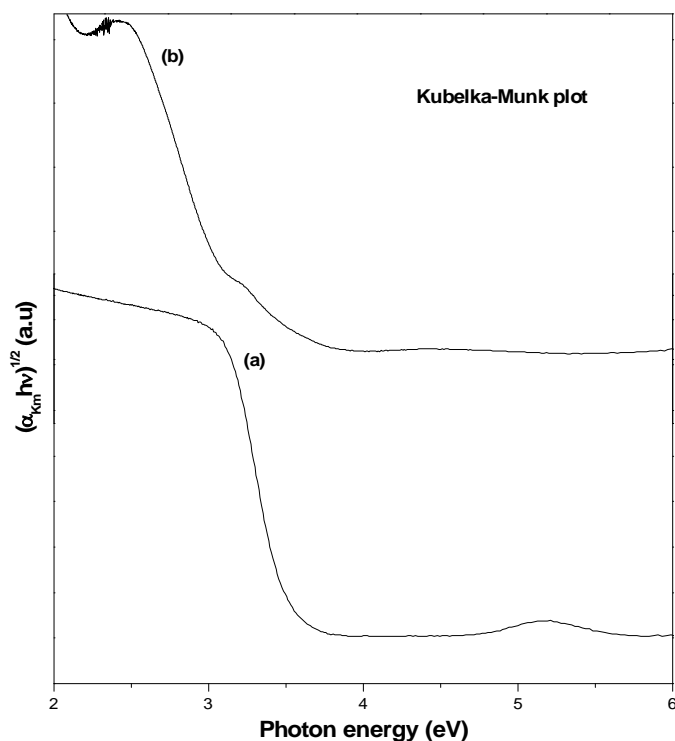


Figure 5: K-M plot for (a) pure and (b) 8% Fe-TiO₂ nanoparticles

Determination of crystallite size (Brus model): The particle sizes of the prepared TiO₂ nanoparticles have been determined from the relationship between band gap shift ($\Delta E_g = E_{g(\text{nano})} - E_{g(\text{bulk})}$) and radius (R) of nanoparticles by using the following expression [16],

$$\Delta E = \frac{\pi h}{2\mu R} - \frac{1.8e}{\epsilon R} + \text{Polarization terms}$$

Where h is Planck's constant and ϵ is the dielectric constant of the semiconductor material. The calculated band gap shift for the anatase TiO₂ ($E_g = 3.58$ eV) is 0.38 eV as compared to bulk anatase ($E_g = 3.2$ eV). However, the band gap shifts were obtained to be 0.40, 0.46, 0.43 and 0.42 eV respectively for 4%, 8%, 12%, & 16% Fe doped TiO₂ nanoparticles. ' μ ' is the reduced mass of the exciton, ' e ' is the electron charge (1.6×10^{-19} C). The shifts in band gap were significantly affected by the reduced mass of exciton and the dielectric constant of the semiconductor [17]. The value of $\mu = 1.63 m_e$, where m_e is the electron rest mass (9.1×10^{-31} Kg) [15]. Since, the optical dielectric constant of bulk titanium dioxide is very large ($\epsilon = 170$), the coulombic and polarization terms in the equation are neglected. The calculated crystallite sizes of the pure and Fe doped TiO₂ (Brus model) are larger than the values obtained from XRD (Sherrer relation), this may be due to aggregation of nanoparticles. The comparison of band gap energies by direct and indirect methods and crystallite size measurement by DRS analysis with XRD are depicted in Table 2.

Table 2: Comparisons of band gap energies and crystallite size measurements for pure and Fe-TiO₂ nanoparticles

Materials	Band gap energy (eV)			Band gap shift (ΔE_g) eV	Crystallite size (nm)	
	$E_g = 1240/\lambda$	Direct	Indirect		XRD (Scherrer)	DRS (Brus model)
Pure TiO ₂	3.58	3.58	3.58	0.38	15.31	24.49
4% Fe-TiO ₂	3.60	-	-	0.40	23.78	23.87
8% Fe-TiO ₂	3.66	3.67	3.67	0.46	17.09	22.26
12% Fe-TiO ₂	3.63	-	-	0.43	11.17	23.03
16% Fe-TiO ₂	3.62	-	-	0.42	11.31	23.29

Conclusions

The pure and iron doped TiO₂ nanocrystals with different doping Fe³⁺ content were successfully prepared via Sol-gel method. The crystallite sizes and lattice parameters were evaluated from XRD measurements. It reveals that the resulting powders were composed of nano-sized spheres. The main discovery of this work was the blue shift of the light absorbance to the range of 344–339 nm. The allowed direct and indirect band gap energies and crystallite sizes were determined by DRS analysis. The DRS result showed that the band gap energy of 8_{wt.}% Fe doped anatase TiO₂ was higher than that of the others. The findings reported herein represent an innovative route to designing higher band gap energy materials that suitable for semiconductor and opto-electronic devices.

REFERENCES

- [1] Seirafianpour, N., Badilescu, S., Djaoued, Y., Bruning, R., Balaji, S., Kahrizi, M., Truong, V. V. 2008. Optical properties of low temperature prepared granular titanium dioxide on a silver substrate. *Thin Solid Films*, 516: 6359–6364.
- [2] Liu, Z., Guo, B., Hong, L., H. Jiang, H. 2005. Preparation and characterization of cerium oxide doped TiO₂ nanoparticles. *J. Phy. Chem. Solid.*, 66: 161–167.
- [3] Shah, S. I., Li, W., Huang, C. P., Jung, O., Ni, C. 2002. *Proc. Natl. Acad. Sci. USA.*, 99: 6482.
- [4] Liqiang, J., Xiaojun, S., Baifu, X., Baiqi, W., Weimin, C., Honggang, F. 2004. The preparation and characterization of La doped TiO₂ nanoparticles and their photocatalytic activity. *J. Solid State Chem.*, 177: 3375–3382.
- [5] Baifu, X., Zhiyu, R., Peng, W., Jia, L., Liqiang, J., Honggang, F. 2007. Study on the mechanisms of photoinduced carriers separation and recombination for Fe³⁺-TiO₂ photocatalysts. *Appl. Surf. Sci.*, 253: 4390–4395.
- [6] Praveen, P., Viruthagiri, G., Mugundan, S., Shanmugam, N. 2013. Structural, optical and morphological analyses of pristine Titanium di-oxide nanoparticles–Synthesized by Sol-gel route. *Spectrochim. Acta A*, doi: <http://dx.doi.org/10.1016/j.saa.2013.09.037>.
- [7] Rajamannan, B., Mugundan, S., Viruthagiri, G., Praveen, P., Shanmugam, N. 2013. Linear and Non-linear Optical studies of Bare and Copper doped TiO₂ nanoparticles via sol-gel technique. *Spectrochim. Acta A*, doi: <http://dx.doi.org/10.1016/j.saa.2013.09.045>.
- [8] Wang, M., Guo, D. J., Li, H. L. 2005. High activity of novel Pd/TiO₂ nanotube catalysts for methanol electro-oxidation. *J. Solid State Chem.*, 178: 1996–2000.
- [9] Zhang, D., 2012. Enhancement of the Photocatalytic Activity of Modified TiO₂ Nanoparticles with Zn²⁺-Correlation between Structure and Properties. *Russ. J. Phys. Chem. A*, 86: 489–494.
- [10] Chauhan, R., Kumar, A., Chaudhary, R. P., 2012. Structural and optical characterization of Zn doped TiO₂ nanoparticles prepared by sol-gel method. *J. Sol-Gel Sci. Technol.*, 61: 585–591.
- [11] Chuan Xu, J., Shi, Y. L., Huang, J. E., Wang, B., Li, H. L. 2004. Doping metal ions only onto the catalyst surface. *J. Mol. Catal. A: Chem.*, 219: 351–355.
- [12] Zhao, W., Bai, Z., Ren, A., Guo, B., Wu, C. 2010. Sunlight photocatalytic activity of CdS modified TiO₂ loaded on activated carbon fibers. *Appl. Surf. Sci.*, 256: 3493–3498.
- [13] Grabmaier, B. C. and G. Blasse, G. 1994. *Luminescent materials*, Springer, Berlin.
- [14] Vijayalakshmi, R., and Rajendran, V., 2012. Synthesis and characterization of nano-TiO₂ via different methods. *Arch. Appl. Sci. Res.*, 4 (2):1183–1190.
- [15] Lin, H., Huang, C. P., Li, W., Ni, C., Ismat Shah, S., Tseng, Y. H. 2006. Size dependency of nanocrystalline TiO₂ on its optical property and photocatalytic reactivity exemplified by 2-chlorophenol. *Appl. Catal. B: Environ.*, 68: 1–11.
- [16] Kathiravan, A. and Renganathan, R. 2009. Photosensitization of colloidal TiO₂ nanoparticles with phycocyanin pigment. *J. Colloid Interface Sci.*, 335: 196–202.
- [17] King, D. M., Du, X., Cavanagh, A. S., Weimer, A. W. 2008. Quantum confinement in amorphous TiO₂ films studied via atomic layer deposition.
